J Mater Sci (2006) 41:8079–8085
DOI 10.1007/s10853-006-0015-x

Development of piezoelectric monomorph actuator using electrophoretic deposition

Y. H. Chen · T. Li · J. Ma

Received: 21 December 2005 / Accepted: 15 March 2006 / Published online: 28 October 2006

Abstract In the present work, investigation of the functional property of piezoelectric graded monomorph actuator systems is presented. The functional graded actuators were fabricated by electrophoretic deposition (EPD) using pure PZT and doped PZT materials. Actuators developed have shown gradual gradient variation in microstructure. It is noted that the trend in microstructural gradient does not represent similar trend in piezoelectric property gradient. The displacement of microstructural graded and both piezoelectric and microstructural graded actuators were measured in the static condition. The latter was also measured under dynamic condition. The results show that the proper gradient distribution of the piezoelectric properties is important to improve the electromechanical performance of the actuator.

Introduction

Piezoelectric bimorphs or unimorphs have been widely applied in many applications, such as positioners, valves, motors and vibration dampers, due to their capability of generating larger displacement compared with the piezo stacks or multilayer actuators [1–4]. However, the bimorphs have the shortcoming of poor interfacial bondings, which may result in the cracking and peeling of the bonding agent in severe conditions and discourages the applications of the actuator [5–8]. A monolithic actuator, called FGM monomorph, has been proposed to solve this problem [9]. The FGM monomorph has a compositional or functional graded over the cross section in order to smooth the stress distribution and minimize the stress peaks. To form the FGM structure, EPD technique was applied in this paper as it was reported as a very effective method to form the functional graded and multilayer ceramic composites [10–12]. In this paper, the effect of compositional and microstructural gradient and piezoelectric property gradient is investigated by comparing the actuators with and without piezoelectric graded. Also, the actuators with piezoelectric graded were investigated on the electromechanical property both in static and dynamic states.

Y. H. Chen (✉) · T. Li · J. Ma
School of Materials Science and Engineering, Nanyang Technological University, Singapore 639798, Singapore
e-mail: chenyh@ntu.edu.sg

Electrophoretic deposition

Characterization of suspension

The initial powders to fabricate FGM monomorphs involve two kinds of ceramics: $0.95Pb(Zr_{0.52}Ti_{0.48})O_3 \cdot 0.03BiFeO_3 \cdot 0.02Ba(Cu_{0.5}W_{0.5})O_3 + 0.5wt\%MnO_2$ (PZT1) and $Pb(Zr_{0.52}Ti_{0.48})O_3$ (PZT0). Both powders were prepared using conventional oxide mixing method. The raw oxide powders were calcined at 750 and 800 °C for 2 h for PZT1 and PZT0, respectively. Then they were ball-milled at 150 rpm for 8 h. After that the particle sizes of the powders and zeta potential of the suspensions were measured using acoustic spectrometer DT-1200 (Dispersion Technology, Inc.) and ZetaPlus (Brookhaven Instruments, USA), respectively.

Figure 1 shows the result of the particle size distribution. It can be seen that both powders possess similar average size of particles. This will help to form a uniform structure during the electrophoretic deposition. Figure 2 shows the zeta potentials of the two powders in ethanol as a function of pH. 10% HNO_3 was added to the suspension to adjust pH value. A pH between 4 and 5 where the zeta potential is maximum is noted to be optimum for both powders and hence this ionic concentration was selected to perform the later EPD process.

Procedure of electrophoretic deposition

Electrophoretic deposition was performed using the setup as shown in Fig. 3. The deposition cell, made of a stainless steel cup with a diameter of 30 mm, works as the anode. The cathode is the graphite plate substrate with thickness of 1 mm, and width of 5 mm. The suspension was stirred with a magnetic stirrer at the speed of 180 rpm/min to avoid sedimentation of the powder particles during the deposition process. The two powders were mixed into different ratios and suspensions were prepared accordingly in ethanol. The powder concentration in the suspension was 50 g/l and the suspension pH was controlled to be 4.6 by adding 10% HNO_3. To fabricate the monomorph actuator, the suspensions of various compositions were deposited consecutively to the cathode graphite substrates with a uniform layer thickness driven by the electric field. The initial voltage used was 50 V. And the applied voltage was increased with 25 V after every additional layer was deposited, until a final thickness around 0.4 mm was achieved. Under this voltage profile, the deposited mass as a function of time is shown in Fig. 4. It can be seen that the deposited mass increases almost linearly with the deposition time. Therefore, the thickness of the layers can be well controlled by adjusting the deposition time and also the applied voltage to the suspension.

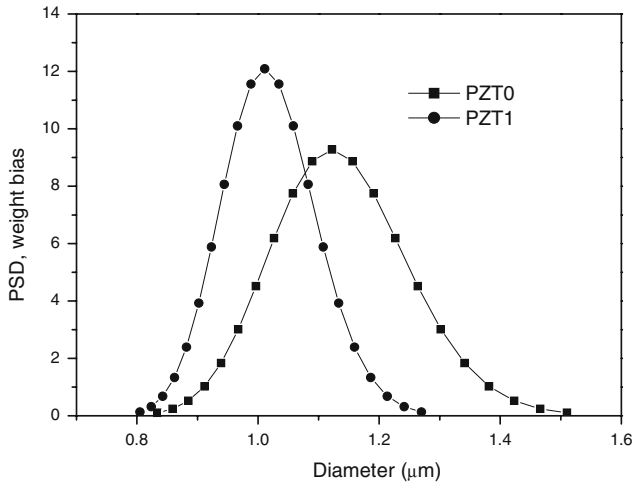

Fig. 1 Particle size distributions of PZT0 and PZT1 powders

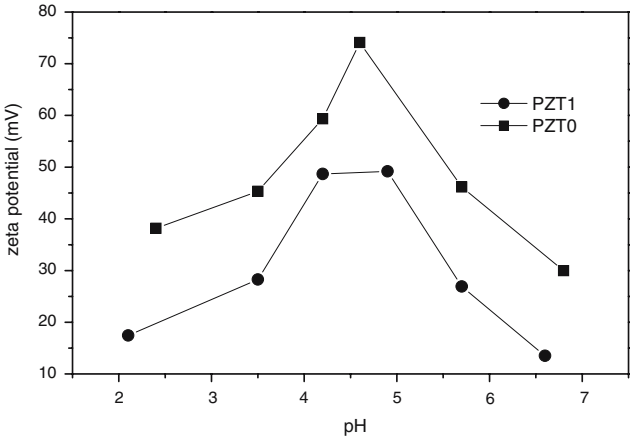

Fig. 2 Zeta potential versus pH value of PZT0 and PZT1 suspensions

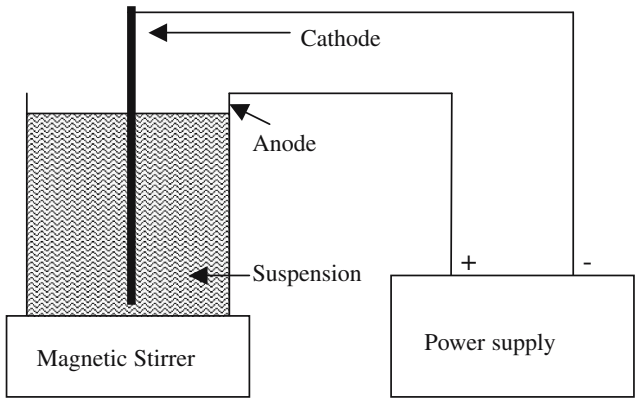

Fig. 3 Schematic drawing of electrophoretic deposition system

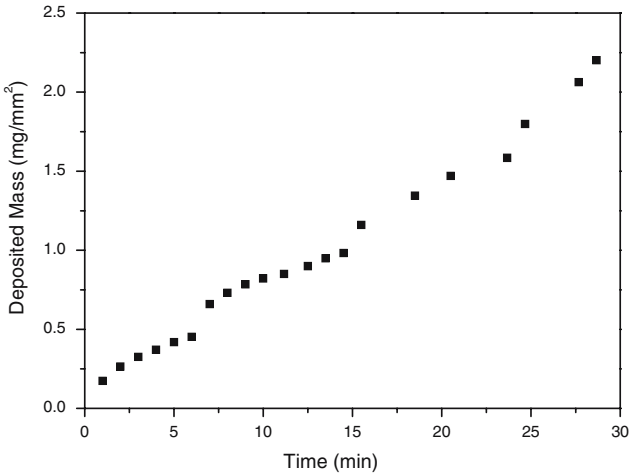

Fig. 4 Deposited mass as a function of deposition time for a 4-layer system

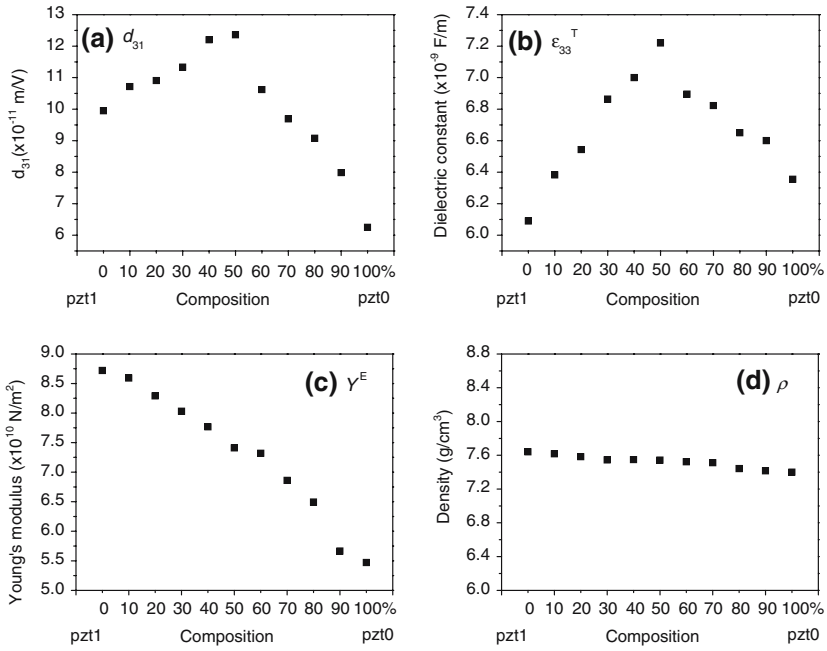

Fig. 5 Variation of material properties as a function of composition

Sintering and poling

After deposition, the deposits were dried for 12 h and sintered at 1,100 °C for 1 h in Pb rich environment. The deposits were then cut and ground to the desired shape and dimensions, and poled in silicone oil at 100 °C for 30 min under an electric field of 2 kV/mm for the subsequent characterization.

Material composition of the actuators

To study the properties of each composition, eleven compositions with the mixture of PZT1 and PZT0 from 0 to 100% PZT0 were prepared and characterized on the piezoelectric constant d_{31}, dielectric constant, ε_{33}^{T} Young's modulus Y^{E}, and density ρ, using the electrophoretic deposited samples. The density was measured using a Densimeter MD-200S; the dielectric constant, Young's modulus and piezoelectric constant were measured using the conventional resonance method with HP 4194A Impedance/Gain-Phase Analyzer. The distribution of the eleven material properties as a function of PZT0 content is shown in Fig. 5. It can be seen that d_{31} increases first with the increase of the PZT0 content, then reaches maximum around 60% to 50% of PZT0, and finally decreases almost linearly. The dielectric constant varies in a similar trend. However, the Young's modulus and density decrease monotonously with the increase of the PZT0 content. Due to the fact that piezoelectric constant d_{31} is the key factor that determines the displacement of the piezoelectric actuator, based on the distribution of d_{31} as a function of composition, three systems are identified: in the 2-layer system, there are 40 and 100% PZT0 content in each layer respectively; Similarly in the 4- and 6-layer systems, the PZT0 content in each layer is 40, 60, 80, 100% and 40, 50, 60, 70, 80, 90%, respectively. In this range, the dielectric constant, Young's modulus and density also vary in the same manner. As a comparison, a 5-layer system was also selected, in which the PZT0 content in each layer mixture is 0, 25, 50, 75, and 100%, respectively. Different from the previous systems, the 5-layer system does not show a one-direction gradient change in the piezoelectric properties.

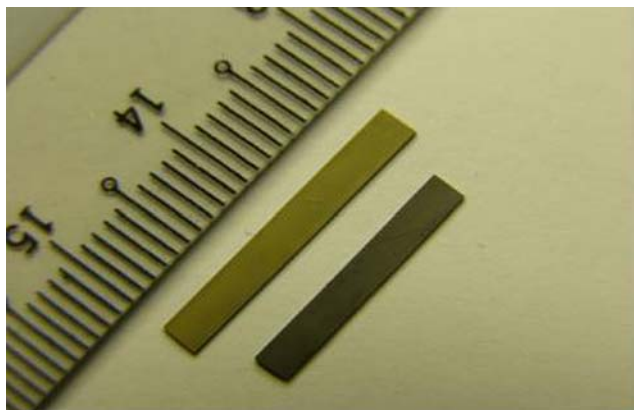

Fig. 6 Photograph of monomorph after sintering

Physical properties

In this section, the monomorphs of different systems were studied on physical properties. Figure 6 shows examples of the monomorph after sintering. The uniform structure was observed. Due to the variation of composition, the upper and lower surfaces show different colors. The monomorph were then smashed for XRD characterization. And the cross section was also observed using SEM.

Figure 7 shows the XRD patterns of the 2-, 4-, 6- and 5-layer systems, respectively. The expected perovskite structure was confirmed to be presented in all the four systems. Even varying in composition, no significant difference in phase structure was revealed from this XRD measurement. The microstructures of the cross section of the 2-, 4-, 6- and 5-layer system are shown in Figs. 8–11, respectively. It can be seen that, for all the systems, the gradient variation in grain size is clearly shown. The side with more PZT1 content in the actuator shows larger grain size than the other side. The grain size changes gradually over the cross section. This variation of grain size is attributed to the effect of dopants added in PZT1, which promoted grain growth during sintering. However, it is noted that even the grain size monotonously increases with more PZT1 content, but the piezoelectric properties do not follow the same trend as shown in Fig. 5, where both piezoelectric and dielectric constants show peak values. This indicates that a microstructure gradient does not necessarily mean a piezoelectric property gradient.

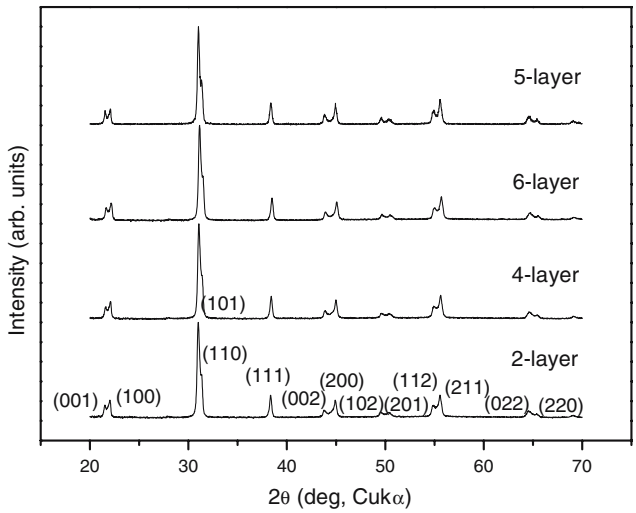

Fig. 7 XRD patterns of the 2-, 4-, 6- and 5-layer monomorphs

Electromechanical properties

The electromechanical property—electric field induced bending displacement—of the developed monomorph actuators was measured using the system as shown in Fig. 12 both under static and dynamic conditions. The system consists of a power supply, a vibraplane, a MTI2000 fotonic sensor and the sample. For the static measurement, the power supply is the RT6000HVS ferroelectric tester, which generates a triangle signal and applied to the electrodes on the top and bottom surfaces of the actuators. For dynamic measurement, the power supply is the FG300 function generator,

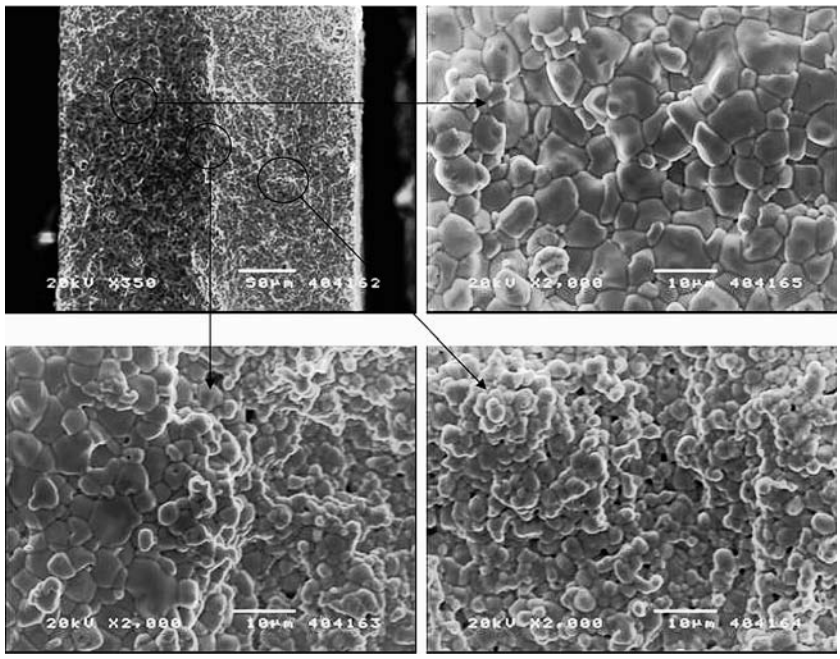

Fig. 8 Gradient variation of microstructure of 2-layer system FGM monomorph over cross section

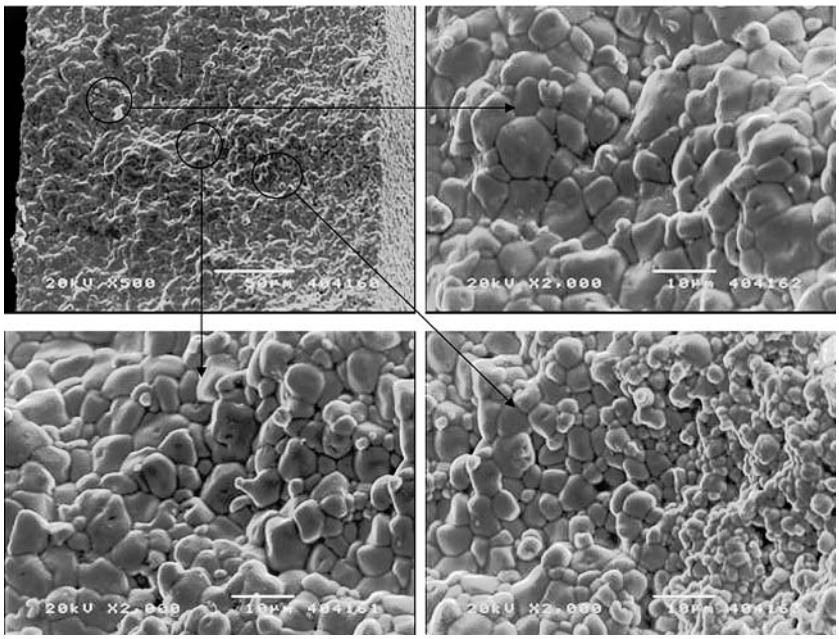

Fig. 9 Gradient variation of microstructure of 4-layer system FGM monomorph over cross section

which produces sinusoidal waves. The actuator was fixed to the vibraplane and measured under Clamped-Free boundary condition. The displacement at the tip of the actuator was measured using the fotonic sensor.

Figure 13 shows the static bending displacement hysteresis loop. The displacement is measured at 2.5 Hz. The dimensions of the four systems from 2-, 4-, 6- to 5-layer are 14.5-2.94-0.23, 15.0-2.62-0.26, 15.0-2.55-0.34, and 15.0-3.00-0.30 (mm), respectively. Displacements of approximately 19.39, 12.13, 5.29 and 3.98 μm were achieved at a voltage of 100 V for the four systems. For the 2-, 4- and 6-layer system, which has a one directional gradient piezoelectric constant distribution over the cross section, the bending displacement tends to decrease with the increase of the number of layers. However, all the three systems generate a larger

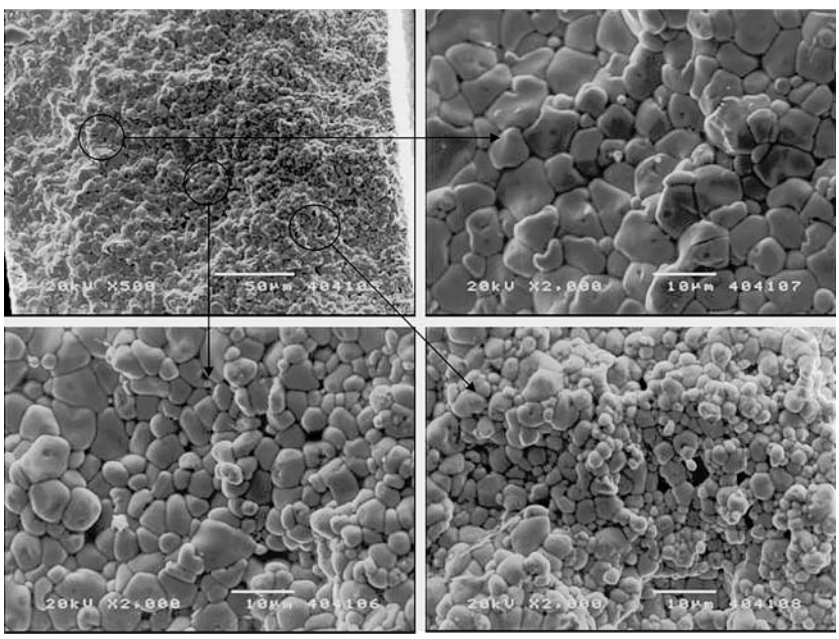

Fig. 10 Gradient variation of microstructure of 6-layer system FGM monomorph over cross section

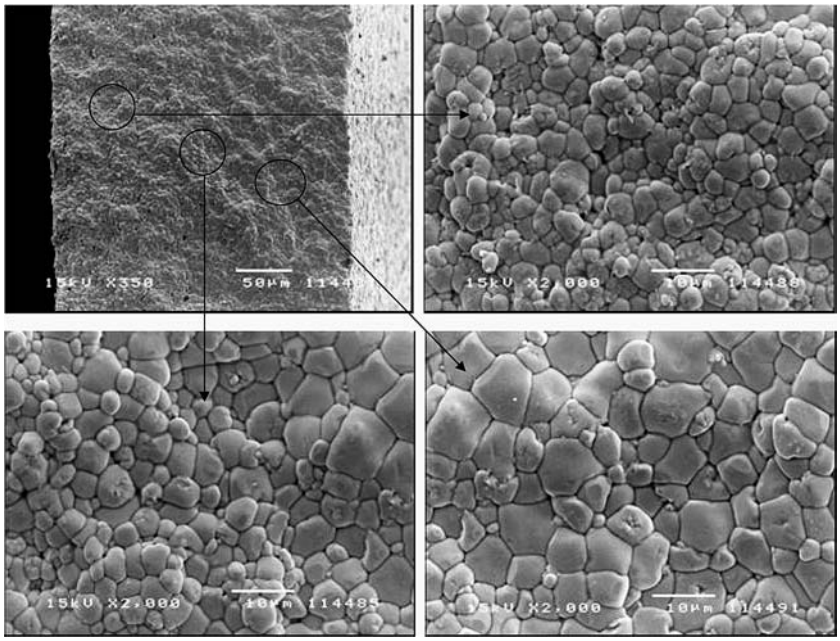

Fig. 11 Gradient variation of microstructure of 5-layer system FGM monomorph over cross section

displacement than the 5-layer system, which does not has a gradient distribution of piezoelectric properties over the cross section. This indicates that a proper gradient piezo material property distribution over the cross section is essential to improve the electromechanical properties of the actuator since 2-, 4- and 6-layer systems are improved over 5-layer system.

Figure 14 shows the behavior of the 2-, 4- and 6-layer monomorphs in the dynamic state. A sinusoidal wave was applied through the function generator at 1 Vp-p. The studied frequency range is from 100 to 700 Hz. The bending displacement is frequency dependent. At certain frequency, the magnitude of displacement reaches a peak value. This frequency is the so-called resonant frequency. According to the conventional Euler–Bernoulli beam theory [13], at resonance, a Clamped-Free vibration monomorph will show the deformed shape $Y(x)$ as described in the following equation

$$Y(x) = \cosh \lambda x - \cos \lambda x + \alpha(\sinh \lambda x - \sin \lambda x) \quad (1)$$

where λ and α are constants. For the first order vibration, α is –0.73; and λl is 1.88, l is the length. x is the position from 0 to l.

From Fig. 14, it can be seen that the magnitude of the resonant displacement follows the same trend as

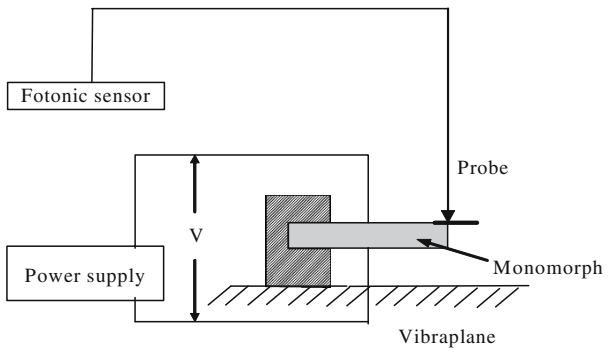

*Power supply: RT6000 HVS ferroelectric tester for static measurement and FG300 function generator for dynamic measurement

Fig. 12 Setup for displacement measurement

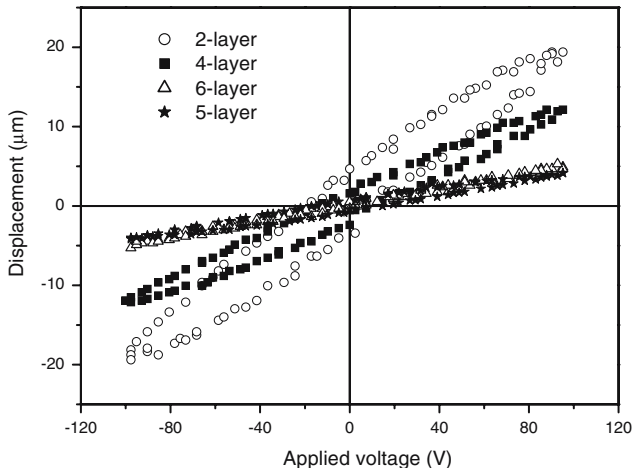

Fig. 13 Displacement hysteresis loops of the 2-, 4-, 6- and 5-layer monomorph

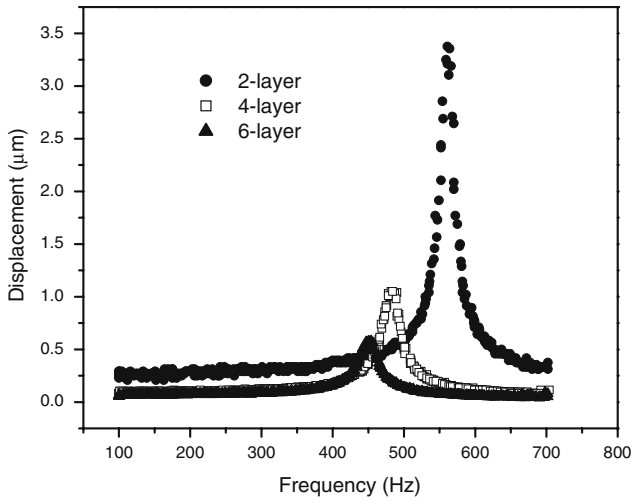

Fig. 14 Frequency dependence of the bending displacement of the 2-, 4- and 6-layer monomorph

that in the static measurement, i.e., the 2-layer system has the largest dynamic displacement, followed by 4- and 6-layer systems. Therefore, increasing the number of layers will reduce the displacement of the actuator both under static and dynamic conditions. For applications where large displacement is essential, less layer system is preferred at the expense of smooth stress distributions [14].

Conclusions

Four monomorph actuators, with and without monotonic variation of piezoelectric properties over the cross section, were successfully fabricated using EPD. Both types of the actuators exhibit gradient microstructure. However, the actuators with piezoelectric gradient show larger bending displacement than the non-piezoelectric-gradient actuator. The proper gradient distribution of the piezoelectric properties over the cross section is important for the improvement of electromechanical properties of the actuators. For the actuators with monotonic variation of piezoelectric properties over the cross section, the bending displacement decreases with the increase of the number of the layers both in static and dynamic states.

References

1. Jones DJ, Prasad SE, Wallace JB (1996) Key Eng Mat 122–124:71
2. Uchino K (1993) MRS Bulletin 42
3. Niezrechi C, Brei D, Moskalik A (2001) The Shock and Vibration Digest 33:269
4. Uchino K (1998) Smart Mater Struct 7:273
5. Uchino K (1997) In: Tuller HL (eds). Piezoelectric Actuators and Ultrasonic Motors. Kluwer Academic Publishers, Boston, p. 140
6. Smits JG, Dalke SI, Cooney TK (1991) Sensors and Actuators A 28:41
7. Zhu XH, Meng ZY (1995) Sensors and Actuators A 48:169
8. Wu CCM, Kahn M, Moy W (1996) J Am Ceram Soc 79:809
9. Chen YH, Li T, Ma J (2003) J Mater Sci 38:2803
10. Nagai M, Yamashita Y, Takuma Y (1993) J Am Ceram Soc 76:153
11. Ferrari B, Moreno R (1997) J Eur Ceram Soc 17:549
12. Sarkar P, Huang X, Nicholson PS (1992) J Am Ceram Soc 75:2907
13. de Silva CW (1999) Vibration: fundamentals and practice. CRC Press, Boca Raton, p. 299
14. Kouvatov A, Steinhausen R, Langhammer HT (1999) J Eur Ceram Soc 19:1153